PAPER

Flat optical transparent window: mechanism and realization based on metasurfaces

IOP Publishing Journal of Physics D: Applied Physics

J. Phys. D: Appl. Phys. **51** (2018) 074001 (12pp) https://doi.org/10.1088/1361-6463/aaa451

Flat optical transparent window: mechanism and realization based on metasurfaces

Huijie Guo[1], Jing Lin[1], Meng Qiu[1], Junxia Tian[2], Qian Wang[2], Yue Li[3], Shulin Sun[5], Qiong He[1,4], Shiyi Xiao[3,6] and Lei Zhou[1,4,6]

[1] State Key Laboratory of Surface Physics, Key Laboratory of Micro and Nano Photonic Structures (Ministry of Education) and Physics Department, Fudan University, Shanghai 200433, People's Republic of China
[2] The Aeronautical Science Key Lab for High Performance Electromagnetic Windows, The Research Institute for Special Structures of Aeronautical Composite AVIC, Ji'nan, Shandong 250023, People's Republic of China
[3] Key Laboratory of Specialty Fiber Optics and Optical Access Networks, Shanghai University, Shanghai 200444, People's Republic of China
[4] Collaborative Innovation Center of Advanced Microstructures, Fudan University, Shanghai 200433, People' Republic of China
[5] Green Photonics and Department of Optical Science and Engineering, Shanghai Engineering Research Center of Ultra-Precision Optical Manufacturing, Fudan University, Shanghai 200433, People's Republic of China

E-mail: phzhou@fudan.edu.cn and phxiao@shu.edu.cn

Received 1 October 2017, revised 12 December 2017
Accepted for publication 28 December 2017
Published 1 February 2018

Abstract

A material exhibiting a wide-band optical transparent window (OTW) with *negligible* transmittance fluctuation is highly desired in various applications, but the conventional approach of stacking multiple transmission-resonant metasurfaces creates undesired amplitude fluctuations within the OTW. In this article, we first establish a coupled-mode theory to understand the inherent physics governing the transmission properties in such systems, based on which we then propose a criterion that can help researchers design structures exhibiting wide-band OTWs with diminished transmittance fluctuations. Compared to a brute-force optimization method, our approach is much faster and physically intuitive. As an illustration of our theory, we design a four-layer structure (with a total thickness of 36 mm) through solving the proposed criterion, and experimentally demonstrate that it exhibits a flat OTW within the 3.7–5 GHz range, with transmittance fluctuations smaller than 10 percent. Our findings can stimulate the design of artificial structures exhibiting the desired shapes of transmission windows fitting applications in different frequency regimes.

Keywords: transparent window, metasurface, resonance-induced transparency, Fano resonances, coupled-mode theory

S Supplementary material for this article is available online

(Some figures may appear in colour only in the online journal)

1. Introduction

The matter of making an opaque medium optically transparent has attracted intense attention recently, due to both scientific curiosity and its potential practical applications. In particular, a slab of material that allows only electromagnetic (EM) waves to pass through within a certain frequency band is highly desired in many applications, such as microwave radar radomes [1, 2] and transparent electrodes for solar cells [3, 4]. In these applications, one typically requires the material to exhibit a broad and square-wave-like optical transparent window (OTW), inside which the

[6] Authors to whom any correspondence should be addressed.

transmittance is as high as possible and the transmittance fluctuation is as small as possible. To meet these application requirements, a commonly adopted approach is first to design a metasurface exhibiting a transmission resonance at the target frequency (see figure 1(a)), and then to stack multiple layers of such metasurfaces to form a slab (see figure 1(b)) [5–8]. The core idea of such an approach is to employ the mutual interactions between transmission resonances in different layers to broaden the optical transparency band of the whole system, thus generating a desired OTW with a certain bandwidth.

Despite the great successes already achieved with such an approach [5–8], many issues remain unsolved. For example, directly stacking multilayers with *equal* inter-layer spacers always creates a highly non-flat transmission band in which both the amplitude and the phase of the transmission fluctuate dramatically (compare figures 1(c) and (d)). In fact, a similar issue also occurs in other multilayer optical devices, such as multilayer perfect absorbers [9–12], chiral cascaded metasurfaces [13, 14], and transmission-mode meta-devices with different functionalities (for instance, meta-lenses, beam defectors, and so on) [5–8, 15–18]. Such an inherent problem significantly limits the working bandwidths and performances of these optical elements and devices. Although brute-force numerical optimizations might help in the design of a system with better performance, the computations are very time-consuming, especially for systems with many structural parameters. More importantly, they cannot reveal the underlying physics.

In this paper, we establish a highly efficient approach to the design of a flat-band OTW material based on multilayer metasurfaces. Through analyzing equal-spaced multilayer metasurfaces using the coupled mode theory (CMT) [19, 20], we find that the crucial properties (i.e. the position and bandwidth) of each transmission peak inside an OTW are determined solely by a particular set of model parameters describing both inter-layer near-field couplings and far-field radiations. This motivates us to set up a guideline to design a flat-band OTW where the transmittance fluctuations are suppressed through the appropriate rearrangement of the transmission peaks involved. As a proof of concept, we design and fabricate a microwave OTW material and experimentally demonstrate that it exhibits a square-wave-like OTW within the 3.7–5 GHz range, in which the transmittance is always larger than 80 percent and with transmittance fluctuation less than 10 percent. Our design approach is fast, robust, flexible, and can be applied to realize artificial structures with desired OTW shapes for different applications in different frequency regimes.

Our paper is organized as follows. After briefly describing in section 2 the bottleneck issues faced by the conventional approach, we establish our CMT formalisms to study both single-layer and double-layer systems in sections 3 and 4, respectively, based on which we set up a criterion to design a flat-band OTW material. Section 5 is devoted to an experimental implementation of our approach in the microwave regime, and we conclude our paper in section 6.

2. Issues in conventional approach to design OTW materials

We take a concrete example to illustrate the bottleneck issues encountered by the conventional approach to the design of an OTW material. Without losing generality, here we assume that the unit element of our single-layer metasurface consists of a metallic 'H' surrounded by a metallic square (see figure 1(a)). To illustrate only the key physics, without involving too many complexities, we assume that the metal is a perfect electric conductor (PEC) and that there is no substrate in the structure, in all the analyses performed in sections 2–4. The reason to adopt such a composite microstructure is clear: while the metallic mesh blocks EM waves at most frequencies (below the cut off at ~17 GHz), the local resonance contributed by the metallic 'H' can induce optical transparency at a certain frequency. Figure 1(c) depicts the finite difference time domain (FDTD) simulated transmittance spectrum of such a single-layer metasurface, from which one can find a transmission peak at 6.27 GHz within an opaque background.

We now construct an OTW slab by stacking more layers together. The solid lines in figure 1(d) depict the FDTD simulated transmittance/phase spectra of a slab formed by stacking $N = 4$ such layers (N denotes the number of layers) with equal inter-layer distances. While the coupling between these layers does indeed enlarge the total transmission band, there are strong fluctuations of both amplitude and phase inside the transmission band, especially at the high-frequency edge of the OTW. In fact, such fluctuations cause the OTW bandwidth (defined as the frequency range with transmittance $>80\%$ [18]) to become even narrower (compare the shaded regions in figures 1(c) and (d)). These fluctuations cannot be smoothed out by simply varying the inter-layer distance or adding more layers (see figures 1(e) and (f)). As a result, the useful bandwidths of the OTWs in such systems are quite narrow, being unfavorable for practical applications.

Although in principle one can achieve a flat OTW via brute-force optimizations based on full-wave simulations, such optimizations are extremely time-consuming, especially for systems with a large N. Moreover, such schemes cannot reveal the simple physics governing such inherent fluctuations. In what follows, we develop a new scheme to overcome these issues.

3. CMT formalisms for single-layer metasurfaces

We first establish a CMT framework in order to understand the optical properties of a single-layer metasurface. Obviously, such a system can be well described by a two-port single-mode model, where the 'mode' is contributed by the localized resonance brought by the insertion of the 'H' structure. Based on standard CMT analyses [19, 20], we find that the transmission coefficient through such a system can be generally written as

$$t = t_0 + \frac{d_1 d_2}{\mathrm{i}(f - f_{\mathrm{mode}}) + \Gamma_{\mathrm{mode}}}, \tag{1}$$

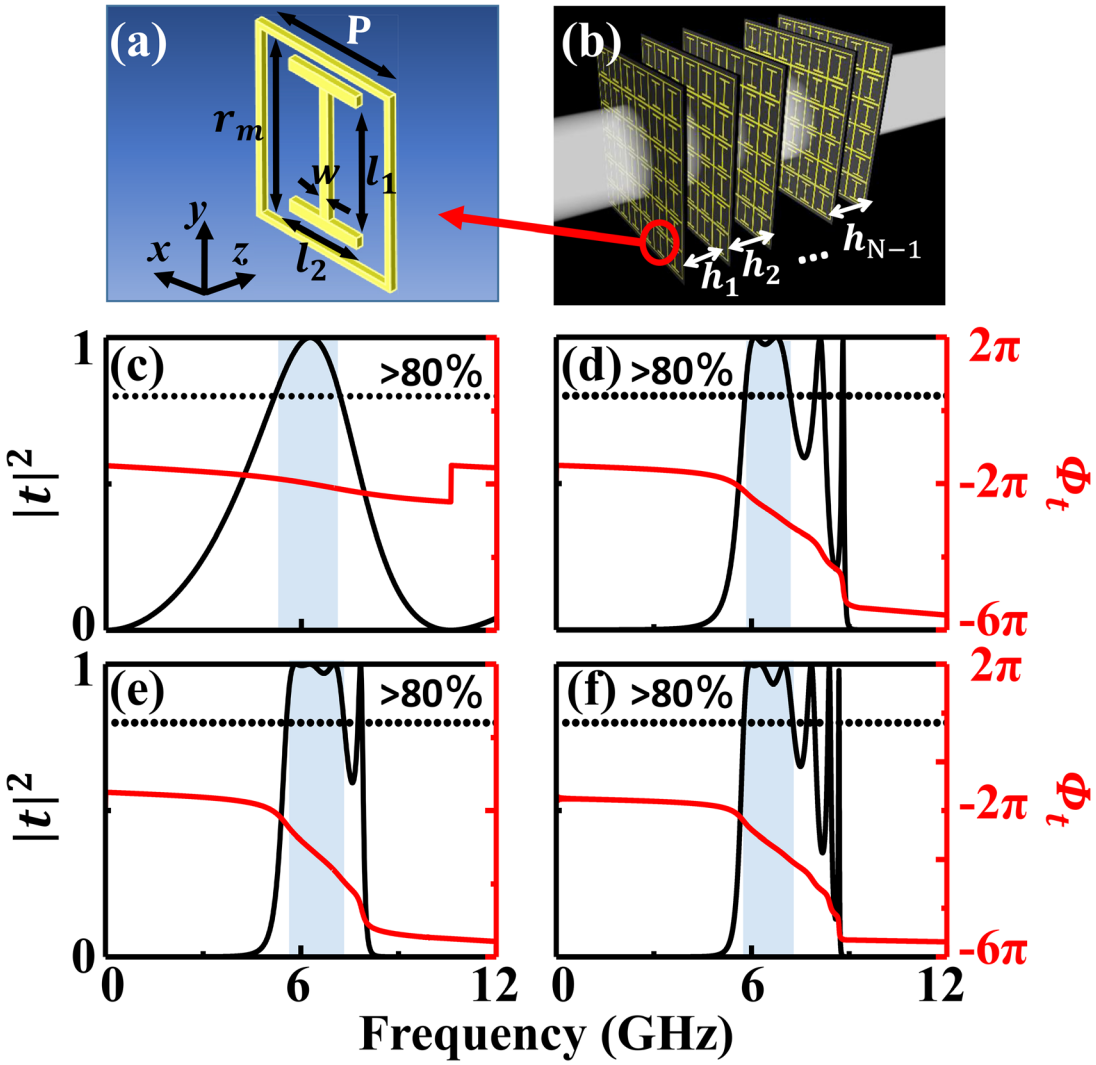

Figure 1. Schematics of (a) unit element of single-layer metasurface with geometric parameters: $P = 9$, $r_m = 8.8$, $l_1 = 7$, $l_2 = 4.5$, $w = 0.5$, all in the unit of mm, and (b) stacked metasurface. Here, the z axis is the propagating direction of the incident wave. Transmittance (black curves) and phase (red curves) spectra of (c) single-layer metasurface, equal-spaced multilayer metasurfaces with (d) $N = 4$ and $h = 4$ mm, (e) $N = 4$ and $h = 8$ mm, and (f) $N = 6$ and $h = 4.8$ mm, where N denotes the number of layers and h denotes the equal inter-layer distance.

where t_0 denotes the transmission coefficient of the background medium, f_{mode} and Γ_{mode} are the frequency and radiation decay rates of the 'mode', and d_1 and d_2 denote the couplings between the localized mode and the two external ports. Here, the absorption-generated decay rate has been neglected, since there is no ohmic loss in our model structure. We note that d_1, d_2 are not independent parameters. Symmetry argument and energy conservation tell us that $d_1 = d_2$ and $\Gamma_{\text{mode}} = (|d_1|^2 + |d_2|^2)/2$ [19, 20]. Further considering the time-reversal symmetry, we note that the phases of these two parameters can be determined by the optical responses (t_0 and r_0) of the background medium (see the appendix for derivations).

Special attention must be paid to the optical responses (t_0, r_0) of the background medium. At first glance, one may think that the background medium would simply be the metallic mesh alone, which exhibits a Drude-like optical response. However, a more careful analysis indicates that such a picture is not valid since it completely overlooks the strong near-field coupling between the metallic mesh and the metallic 'H'. With such near-field (NF) coupling taken into account, we find that the background medium is better characterized by a Lorentz-like response $t_0 = 1 - \frac{\Gamma_0}{\mathrm{i}(f - f_0) + \Gamma_0}$, with f_0 and Γ_0 being the resonance frequency and the radiation decay rate of the 'dressed' background medium[7]. Collecting all these facts, we have altogether four free parameters (f_0,f_{mode},Γ_0 and Γ_{mode}) with which to determine t (see equation (1)). A similar conclusion can be drawn for the reflection coefficient (r).

The solid curves in figures 2(a) and (b) are the best fitted CMT spectra with fitting parameters $f_0 = 3.11$, $\Gamma_0 = 13.08$, $f_{\text{mode}} = 6.8$, and $\Gamma_{\text{mode}} = 2.22$, all in the unit of GHz. Perfect agreement is noted between the CMT spectra and the simulated ones. We emphasize that we can *not* fit the FDTD

[7] Field patterns of 'dressed' mode and 'dressed' background can be found in section 1 of supplementary data.

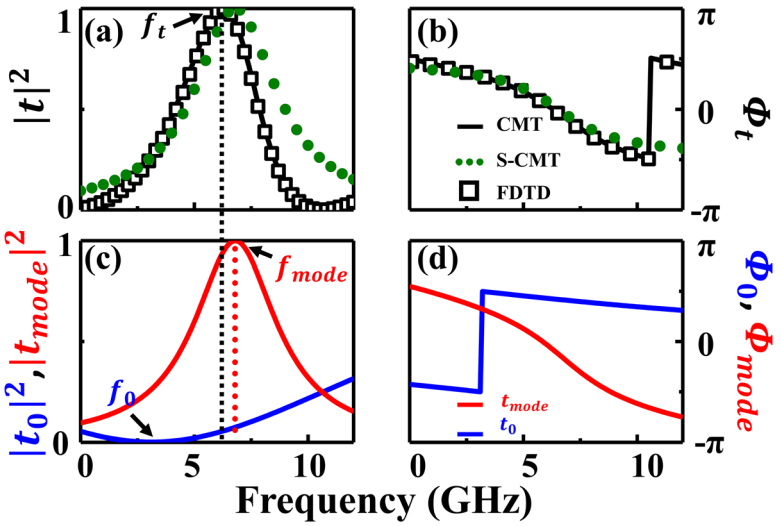

Figure 2. (a) Transmittance and (b) phase spectra of the single-layer metasurface computed by FDTD simulations (black symbols), CMT model (black lines), and simplified CMT mode (green dots). (c) Transmittance and (d) phase spectra of 'background' (blue curves) and 'mode' (red curves) in the CMT model.

spectra if we set $f_0 = 0$ (i.e. assuming a *bare* background), due simply to the argument presented in the above paragraph. In addition, the resonance frequency of the 'mode' (6.8 GHz) differs from that of a bare metallic 'H' (which is about 10.3 GHz), which reinforces our argument that both the 'mode' and the background are 'dressed' states. We note that such a mode-hybridization effect strongly depends on the wave function overlapping between two original bare modes. When the mode associated with 'H' exhibits a high quality (Q) factor, such mode-hybridization effect becomes weak, since the eigen field of the bare 'H' mode is strongly localized at the near-field region of 'H' and does not overlap significantly with that of the mesh. Finally, we note that $\Gamma_0 \gg \Gamma_{\text{mode}}$, which is reasonable, since the background medium is predominantly dictated by the metallic mesh exhibiting a very low Q factor. With equation (1) at hand, we can analytically solve the equation $|t| = 1$ to get the transparent frequency as $f_t = (\Gamma_0 f_{\text{mode}} + \Gamma_{\text{mode}} f_0)/(\Gamma_0 + \Gamma_{\text{mode}})$. The position of f_t is labeled as a dashed line in figure 2(a), agreeing well with the peak position in the FDTD simulated spectra. The physics governing such induced transparency is the Fano effect [21–25]. At the frequency f_t, backward scatterings from the 'background' and the 'mode' destructively interfere with each, leading to perfect transparency. We note that in principle, f_t differs from f_{mode}, although they are highly correlated with each other. While this is a typical characteristic of the Fano effect, such a discrepancy also adds complexities to our future discussions, since we can *not* directly relate the observed optical transparencies with certain local 'modes' inside the structure.

Fortunately, in the limit of $\Gamma_0/\Gamma_{\text{mode}} \to \infty$, we do have $f_t \to f_{\text{mode}}$, indicating that the transmission peak frequency can be well approximated by the resonant frequency of the embedded 'mode'. Such a limit can be approached when the embedded 'mode' exhibits an extremely high Q factor (very small Γ_{mode}), which is not the case here since it is not favorable for the creating of a flat OTW. Meanwhile, another possible solution is $\Gamma_0 \to \infty$, which is the case studied here. Physically, $\Gamma_0 \to \infty$ means that the background is extremely opaque ($t_0 \to 0$), and thus only at the vicinity of the 'mode' can the system have enough strength to induce optical transparency. The t_0 spectrum depicted in figure 2(c) indicates that we do indeed have a very opaque background. Under this limit, equation (1) is approximated as $t \approx -\mathrm{i}\Gamma_{\text{mode}}/(f - f_{\text{mode}} - \mathrm{i}\Gamma_{\text{mode}})$, and the spectra calculated by this simplified CMT model (denoted by s-CMT; green dots in figures 2(a) and (b)) have indeed captured those essential features of the studied single-layer metasurface (i.e. the position and bandwidth of the transmission peak), as compared to those obtained by the full CMT model (equation (1)) and the FDTD simulations.

The s-CMT model is important since it sets up a direct link between the transmission characteristics and the 'modes' embedded inside the system. Such inherent connection enables us to understand the physics of the fascinating transmission properties of a multilayer system, by examining the inherent properties of the collective 'modes' generated inside it.

4. Analyzing two-layer systems based on the simplified CMT

We now employ s-CMT to study the multilayer structures, starting from a two-layer coupled system (figure 3(a)). The analysis in last section revealed that each layer supports a dressed localized 'mode'. However, we cannot directly use the CMT parameters ($f_{\text{mode}}, \Gamma_{\text{mode}}$) derived in the last section to model the 'mode' embedded in one layer of the present system, simply because the 'mode' is now in a different environment. Figure 3(b) shows the FDTD simulated transmission spectrum of a two-layer system, but with only one layer having an 'H' structure inserted. The most pronounced difference between figures 2(a) and 3(b) is that now the peak

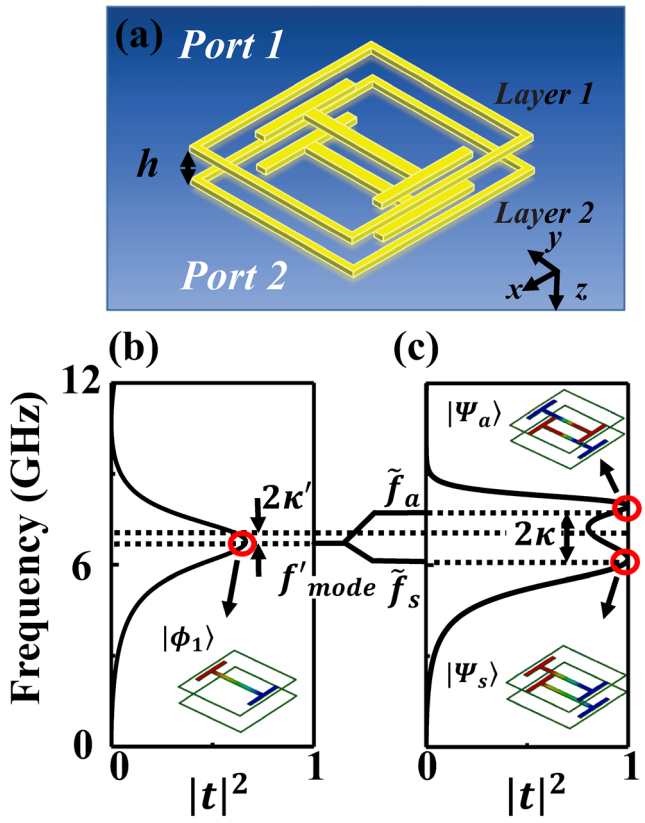

Figure 3. Schematic view of (a) two-layer stacked metasurfaces with inter-layer distance $h = 4.5$ mm. (b) Transmittance spectrum of two-layer metallic mesh with one-layer 'H' shape. Inset depicts the E_z-field pattern with one 'H' structure inserted at layer 1. (c) Transmission of $N = 2$ stacked metasurface with E_z-field pattern for symmetric collective mode $|\Psi_s\rangle$ and anti-symmetric collective mode $|\Psi_a\rangle$. Here, the geometry parameters are the same as in figure 1 and the material is PEC without substrate.

transmittance is not 100 percent (equation (A.6)). Obviously, the difference between two systems is that the 'mode' in a two-layer system radiates *asymmetrically* to two opposite sides, and thus we need to adopt two d parameters to model the couplings of such a mode to two external ports. Based on the s-CMT model (equations (A.5)–(A.6)), we retrieved the fitting parameters for the localized (single-layer) mode located at the first layer: $f'_{\text{mode}} = 6.76$, $d^2_{1,1} = 1.416$, and $d^2_{2,1} = 0.38$, all in units of GHz. We note that f'_{mode} is slightly different than f_{mode} due to the environmental change. Here, $d_{i,j}$ denotes the coupling strength between the 'mode' of the jth layer and the ith external port. Obviously, symmetry arguments tell us that $d_{1,2} = d_{2,1}$ and $d_{2,2} = d_{1,1}$.

We now study the coupled system with 'H' structures added in both layers. FDTD simulations show that two peaks appear in the transmission spectrum, located at different frequencies and with different Q factors (figure 3(c)). This effect is apparently caused by the NF coupling between the two 'modes' being located at two different layers. Obviously, we should employ the multi-mode two-port CMT to study such a system. However, the standard multi-mode CMT [19, 20] always assumes that the involved 'modes' are orthogonal with each other, not the original modes associated with two different layers. To obtain the orthogonal modes of the entire system, we turn off the scattering channels at the moment [25]. Under this condition, we find that the time evolution of the amplitudes of the two original modes at two layers (defined as a_1 and a_2, respectively) are governed by

$$\frac{1}{2\pi}\frac{\mathrm{d}}{\mathrm{d}t}\begin{pmatrix} a_1 \\ a_2 \end{pmatrix} = \mathrm{i}\mathbf{H}\begin{pmatrix} a_1 \\ a_2 \end{pmatrix} = \mathrm{i}\begin{pmatrix} f'_1 + \kappa' & \kappa \\ \kappa & f'_2 + \kappa' \end{pmatrix}\begin{pmatrix} a_1 \\ a_2 \end{pmatrix}, \tag{2}$$

according to the tight binding method (TBM). Here, we have $f'_1 = f'_2 = f'_{\text{mode}}$ according to the system's symmetry. The two parameters, κ and κ', describe the NF coupling between two localized modes and the on-site corrections [26, 27]. Diagonalizing the Hamiltonian matrix using

$$\mathbf{M}\begin{pmatrix} f'_{\text{mode}} + \kappa' & \kappa \\ \kappa & f'_{\text{mode}} + \kappa' \end{pmatrix}\mathbf{M}^{-1} = \begin{pmatrix} \tilde{f}_{\text{s}} & 0 \\ 0 & \tilde{f}_{\text{a}} \end{pmatrix}, \tag{3}$$

with $\mathbf{M} = \frac{1}{\sqrt{2}}\begin{pmatrix} -1 & 1 \\ 1 & 1 \end{pmatrix}$ being the transformation matrix, we get the frequencies (eigenvalues) and the wave functions (eigenvectors) of two orthogonal collective modes

$$\begin{cases} \tilde{f}_{\text{a}} = f'_{\text{mode}} + \kappa' - \kappa, & |\psi_{\text{a}}\rangle = (|\varphi_1\rangle - |\varphi_2\rangle)/\sqrt{2} \\ \tilde{f}_{\text{s}} = f'_{\text{mode}} + \kappa' + \kappa, & |\psi_{\text{s}}\rangle = (|\varphi_1\rangle + |\varphi_2\rangle)/\sqrt{2} \end{cases}, \tag{4}$$

where f'_{mode} and $|\varphi_{1(2)}\rangle$ is used to denote the wave functions of the 1th (2nd) single-layer mode, and $\tilde{f}_{\text{a(s)}}$ and $|\psi_{\text{a(s)}}\rangle$ denote the wave functions of anti-symmetric and symmetric collective modes. We note that the tilde ($\sim$) denotes CMT parameters for collective modes and the subscript (a, s) denotes the symmetry of the mode.

The two coupling coefficients (κ, κ') can in principle be obtained by the photonic TBM developed in [27, 28], but here we treat them as two additional fitting parameters. Specifically, we can easily read from the computed transmission spectrum (figures 3(b) and (c)) to get the values of f'_{mode}, $\tilde{f}_{\text{a}}$ and $\tilde{f}_{\text{s}}$, and then retrieve κ, κ' based on equation (4).

Since the wave functions of the collective 'modes' are determined by those of the original single-layer modes (see equation (4)), we can further compute the couplings between the collective modes with external ports. Specifically, defining $\tilde{d}_{i,j} = \langle \text{Port}_i | \psi_j \rangle$ with $j = a, s$ as the coupling coefficients between the ith port and the jth collective mode (describing the radiation damping towards two ports), we find the following matrix equation

$$\begin{pmatrix} \tilde{d}_{1,\text{a}} & \tilde{d}_{2,\text{a}} \\ \tilde{d}_{1,\text{s}} & \tilde{d}_{2,\text{s}} \end{pmatrix} = \mathbf{M}\begin{pmatrix} d_{1,1} & d_{2,1} \\ d_{1,2} & d_{2,2} \end{pmatrix}, \tag{5}$$

to relate $\tilde{d}_{i,j}$ with $d_{i,j} = \langle \text{Port}_i | \varphi_j \rangle$ describing the coupling strengths between the original localized modes with external ports. Since $d_{i,j}$ are known from studying the single-mode properties, we can use equation (5) to calculate the damping parameters $\tilde{d}_{i,j}$.

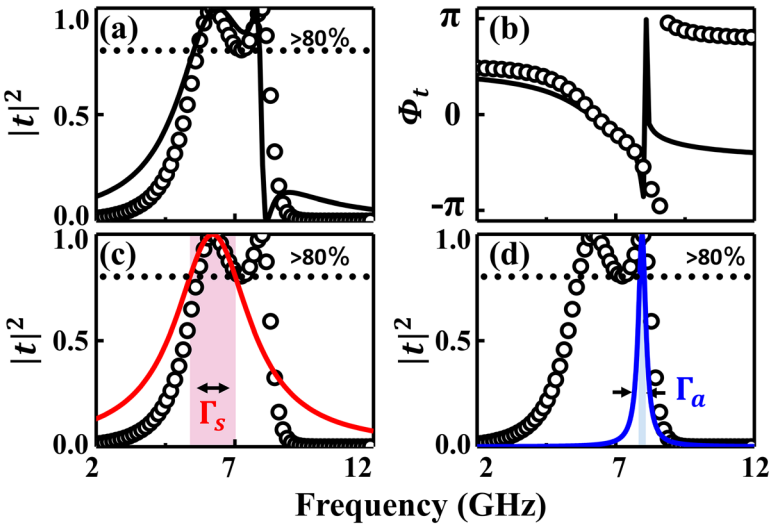

Figure 4. (a) Transmittance and (b) phase spectra of $N = 2$ stacked metasurfaces with $h = 4.5$ mm, where the symbols denote the numerical calculated spectra and the curves denote the fitting CMT spectra. Bandwidth of collective (c) symmetric and (d) anti-symmetric mode fit the simulated spectra very well.

Now we have everything ready to use the standard two-mode, two-port CMT to analyze the transmission coefficient of the two-layer system. Still assuming that the background is extremely opaque ($\Gamma_0 \to \infty$), which is reasonable in such multilayer systems with more mesh layers, we find from the standard CMT that the transmission coefficient can be approximately expressed as

$$t \approx \frac{\tilde{W}_\mathrm{a}\tilde{d}_{1,\mathrm{s}}\tilde{d}_{2,\mathrm{s}} + \tilde{W}_\mathrm{s}\tilde{d}_{1,\mathrm{a}}\tilde{d}_{2,\mathrm{a}} + \tilde{W}_\mathrm{s}\tilde{W}_\mathrm{a}\tilde{X}(\tilde{d}_{1,\mathrm{s}}\tilde{d}_{2,\mathrm{a}} + \tilde{d}_{2,\mathrm{s}}\tilde{d}_{1,\mathrm{a}})}{\tilde{W}_\mathrm{s}\tilde{W}_\mathrm{a} - X^2}, \tag{6}$$

with $\tilde{W}_j = i(f - \tilde{f}_j) + \tilde{\Gamma}_j$ $(j = s, a)$ and $\tilde{d}_{i,j}$ defined in equation (5). $\tilde{X}$ and $\tilde{\Gamma}_j$ are not independent parameters and are determined by the parameters $\tilde{d}_{i,j}$ through $\tilde{X} = -(\tilde{d}^*_{1,\mathrm{s}}\tilde{d}_{1,\mathrm{a}} + \tilde{d}^*_{2,\mathrm{s}}\tilde{d}_{2,\mathrm{a}})/2$ and $\tilde{\Gamma}_j = \left(|\tilde{d}_{1,j}|^2 + |\tilde{d}_{2,j}|^2\right)/2$, according to the elegant arguments of time-reversal symmetry and energy conservation [19, 20]. Therefore, the only fitting parameters in equation (6) are κ, κ', which are found as $\kappa = -0.875$ GHz and $\kappa' = 0.315$ GHz based on careful fitting.

Putting all the model parameters into equation (6), we calculated the transmission spectrum based on equation (6) and depict the obtained results in figures 4(a) and (b). Very good agreement is found between the CMT-fitted spectra and the full-wave simulated ones. The π-phase difference in the frequency regime $f > 8$ GHz is not crucial since the transmittance is nearly zero here. The discrepancy might be caused by our opaque background assumption.

We note that equation (6) is still too complicated to reveal the simple physics. If we neglect the far-field interaction between EM waves radiated from two orthogonal modes (i.e. $\tilde{X} = 0$), equation (6) can be further simplified as $t \approx \tilde{d}_{1,\mathrm{s}}\tilde{d}_{2,\mathrm{s}}/\tilde{W}_\mathrm{s} + \tilde{d}_{1,\mathrm{a}}\tilde{d}_{2,\mathrm{a}}/\tilde{W}_\mathrm{a}$, which describes the optical responses of two *independent* oscillators. Such an assumption is valid at frequencies approaching one of the resonances. To show how powerful our approach is, we have used the formulas

$$t_j \approx \frac{\tilde{d}_{1,j}\tilde{d}_{2,j}}{\tilde{W}_j} = \frac{\tilde{\Gamma}_j}{\mathrm{i}(f - \tilde{f}_j) + \tilde{\Gamma}_j}, \qquad j = s, a \tag{7}$$

to separately calculate the transmission spectra contributed by the symmetrical ($j = s$) and anti-symmetrical ($j = a$) modes, and have plotted them in figures 4(c) and (d). We find that the results obtained with equation (7) are in excellent agreement with full-wave simulations at the vicinities of those peaks, indicating that our model can well capture the essential physics of the 'modes' in the coupled system. In particular, the two parameters $\tilde{f}_j$ and $\tilde{\Gamma}_j$ precisely describe the position and the bandwidth of the jth transmission peak.

Such excellent agreements suggest that we can 'control' the peaks (position and Q factor) inside the OTW, based on the analytical expressions derived in our s-CMT model. The positions of these peaks are determined by the NF coupling through equation (4). Meanwhile, the bandwidths of these transmission peaks, determined respectively by the damping rates of these modes, $\tilde{\Gamma}_\mathrm{s} = \left(|\tilde{d}_{1,\mathrm{s}}|^2 + |\tilde{d}_{2,\mathrm{s}}|^2\right)/2$, and $\tilde{\Gamma}_\mathrm{a} = \left(|\tilde{d}_{1,\mathrm{a}}|^2 + |\tilde{d}_{2,\mathrm{a}}|^2\right)/2$, are dictated by the transformation matrix $\mathbf{M}$ and the single-mode damping parameters $d_{i,j}$. Therefore, one can manipulate the essential properties (position and Q factor) of the generated transmission peaks through *tuning* the NF coupling strengths κ, κ', which are in turn determined by the inter-layer distance h.

The above analysis motivates us to propose the following criterion to create a 'flat' OTW in such a two-layer system:

$$\tilde{f}_\mathrm{a} - \tilde{f}_\mathrm{s} = 2\kappa = \tilde{\Gamma}_\mathrm{a} + \tilde{\Gamma}_\mathrm{s}. \tag{8}$$

The physics of equation (8) is very clear. Now that the half bandwidths of two transmission peaks are determined by their damping rates ($\tilde{\Gamma}_\mathrm{a}, \tilde{\Gamma}_\mathrm{s}$), the best way to suppress the transmission fluctuation is to join two peaks appropriately by setting the inter-peak frequency interval at the same as the sum of their half bandwidths.

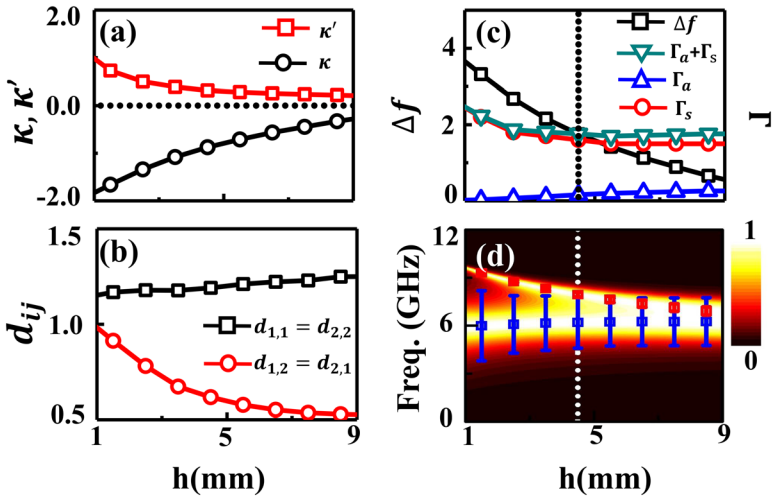

Figure 5. Retrieved CMT fitting parameters of $N = 2$ metasurface. (a) Coupling coefficients (κ, κ'), (b) damping parameters $(d_{i,j})$, and (c) inter-peak frequency interval Δf (black symbols), bandwidths of two peaks $\tilde{\Gamma}_a, \tilde{\Gamma}_s$ (blue and red symbols), and total bandwidths $\tilde{\Gamma}_a + \tilde{\Gamma}_s$ (cyan symbols) as a function of inter-layer distance. (d) Distance dependence of transmittance spectra computed by FDTD simulations, where the symbols and error bar denote the resonating frequencies $(\tilde{f}_j)$ and radiation decay rates $(\tilde{\Gamma}_j)$ of $j = a$ (red) and $j = s$ (blue) mode calculated by CMT analysis.

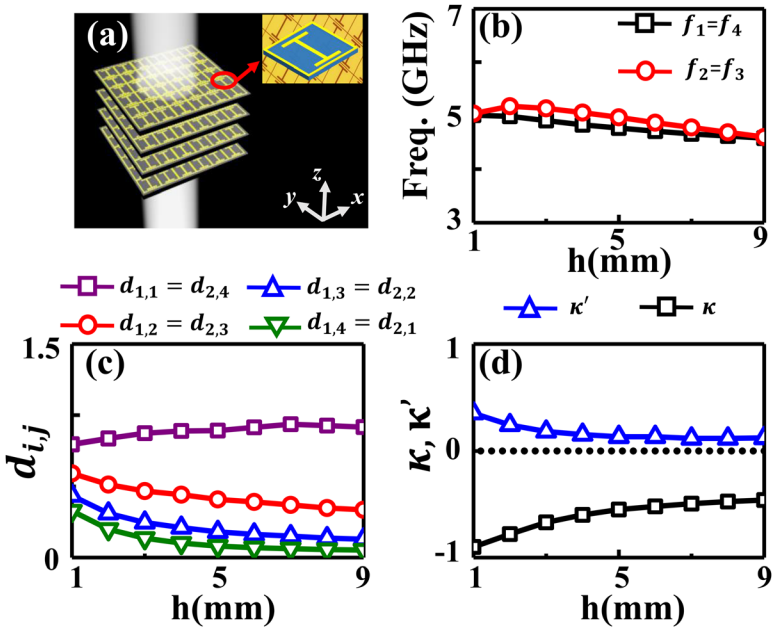

Figure 6. (a) Schematics of the $N = 4$ system. Here, each single-layer metasurface has a 0.5 mm thick substrate with $\varepsilon_r = 4.3$, and the building block structure is depicted in the inset. (b) Frequencies, (c) radiation decay rates, and (d) coupling coefficients of the single-layer 'modes' as a function of inter-layer distance.

To check the validity of the criterion equation (8), we repeated the s-CMT analyses on a series of two-layer systems with different inter-layer distance h, and retrieved the corresponding CMT parameters in different cases. Figures 5(a) and (b) depict how the retrieved CMT parameters vary against h. It is clearly seem from figure 5(a) that both κ and κ' decrease dramatically as h increases, which is reasonable, since both of them depend on the wave-function overlapping of two localized modes. Therefore, tuning h can significantly change the NF coupling coefficients κ and κ', which in turn control both the inter-peak frequency interval Δf and the bandwidths of two peaks $(\tilde{\Gamma}_a, \tilde{\Gamma}_s)$, as shown in figure 5(c). In particular, we can find an inter-layer distance h to satisfy equation (7) (see the dashed line in figures 5(c) and (d)). At this particular case, the two transmission peaks do indeed start to joint together appropriately, forming a flat OTW as shown in figure 5(d), where the FDTD simulated transmission spectra for different values of h are depicted. Such a nice agreement unambiguously justifies our proposed criterion equation (7).

We note that the agreement between the s-CMT results and the FDTD spectra is not surprising for the present two-layer system, since the CMT model parameters are derived from the FDTD simulated spectra. However, the physical

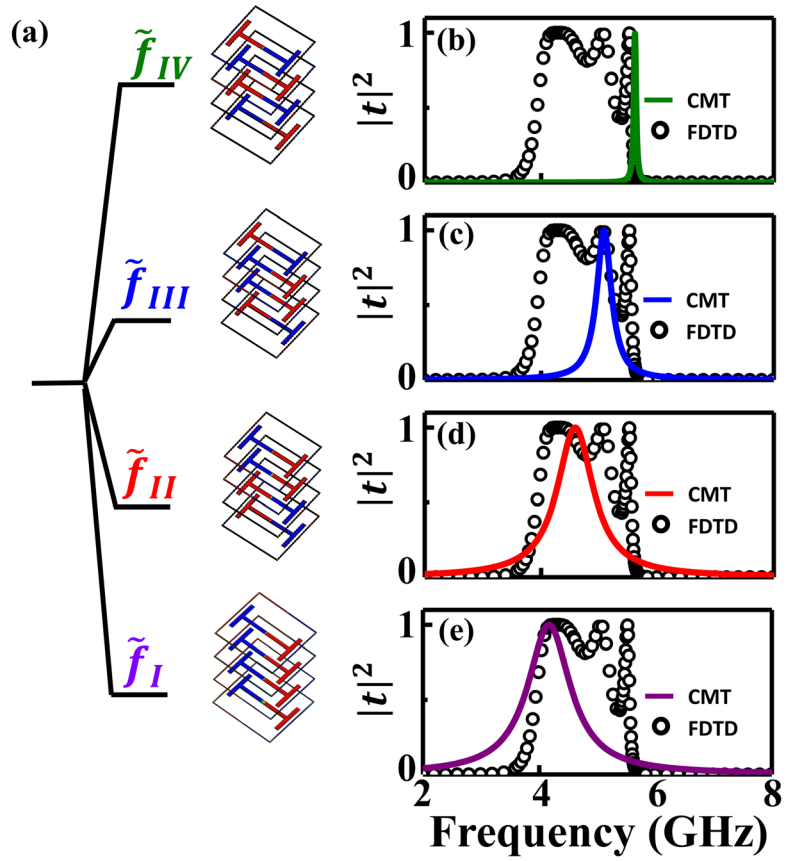

Figure 7. (a) Four collective modes of the $N = 4$ stacked system with equal inter-layer distance of 8 mm. (b)–(e) FDTD-simulated transmission spectra (symbols) and the s-CMT calculated transmission spectra dictated by four collective modes (curves) in the four-layer system.

understanding obtained from the above analyses is very important, and can provide us with a guideline for the design of a flat-band OTW material based on systems with more layers. Moreover, in the two-layer case, the dependence of the half bandwidth $(\tilde{\Gamma}_a + \tilde{\Gamma}_s)$ on h is weak (see figure 5(c)), since the wave functions of two collective modes (see equation (4)) are unchanged irrespective of h, and only the damping parameters $(d_{1,1}, d_{1,2})$ of the original single-layer mode vary against h due to the environmental changes. However, in general systems with more layers, both the inter-peak frequency interval and the half bandwidths can be strongly tuned by the NF couplings, as we shall discuss in the next section.

5. Application to flat-band OTW design

We now take a four-layer system as an example, to illustrate how to design a flat OTW material based on the CMT analyses. To make it realizable in practice, we put the metallic structures (the same as those shown in figure 1(a)) on a 0.5 mm thick dielectric substrate (with $\varepsilon_r = 4.3$, see figure 6(a)). Following the generic strategy described in the last section, we first establish a CMT model in order to understand the nature of all the transmission peaks inside the OTW, and finally obtain an optimized design with which to achieve a flat-band OTW.

The CMT analyses for the four-layer systems are essentially the same as those described in the last section (equations (2)–(7)), with the only difference being that now both the **H** and **M** matrices are 4×4. As a first step, we determine the model parameters for all *independent* single-layer 'modes'. Similar to the two-layer example shown in figure 3, we first calculate the transmission spectra of different *equal-spaced* four-layer systems (with different h) where only one of the four layers has an 'H' structure inserted. Based on this, we can extract the model parameters $(f_i, d_{1,i}, d_{2,i}, i = 1, 2, 3, 4)$ to describe such 'modes' within the CMT. According to the mirror symmetry possessed by the system, we need to consider only two such modes, which are located at the first and the second layers, respectively. We note that these parameters also depend on the inter-layer distance h (see figures 6(b) and (c)), since the 'background environment' changes as we vary h.

We next retrieve the inter-layer coupling constants (κ', κ) for such four-layer systems, still based on *equal-spaced* four-layer systems. We first compute the transmission spectra for a four-layer system (possessing a specific inter-layer distance h) in which only a nearest-neighbor pair of metasurfaces are inserted with 'H' structures (thus supporting the localized 'modes'), and then employ essentially the same technique as in the last section to retrieve the two coupling constants κ, κ'. Our calculations show that κ and κ' sensitively depend only

on h, being quite insensitive to which pairs are studied inside the four-layer system. Figure 6(d) shows how κ and κ' vary as functions of h; it is quite similar to the case of the two-layer system (figure 5(a)).

With all model parameters derived based on *equal-spaced* systems, we can use them to *predict* the transmission behaviors of a *general* four-layer system with *arbitrary* inter-layer distances (i.e. $h_1 \neq h_2 \neq h_3$), without necessarily performing FDTD simulations on these systems. We first use the TBM to obtain all orthogonal collective modes inside such a system. The Hamiltonian matrix is now a 4×4 matrix which can be generally written as

$$\mathbf{H} = \begin{pmatrix} f_1 + \kappa' & \kappa_{12} & 0 & 0 \\ \kappa_{21} & f_2 + \kappa' & \kappa_{23} & 0 \\ 0 & \kappa_{32} & f_3 + \kappa' & \kappa_{34} \\ 0 & 0 & \kappa_{43} & f_4 + \kappa' \end{pmatrix}. \quad (9)$$

Since the inter-layer distances might be non-equal, the inter-layer coupling constants between two adjacent layers (κ_{ij}) are also not necessarily identical. Here, we assume that κ_{ij} is determined solely by the distance between two adjacent layers, following the relationship drawn in figure 6(d). Meanwhile, we assume that the on-site term κ' is the same in different layers and that its value is determined by the average inter-layer distance, following the relationship shown in figure 6(d).

Diagonalizing the matrix $\mathbf{H}$ yields the frequencies (eigenvalues of $\mathbf{H}$[8]) and the eigen-vectors $\tilde{g}_j$ of all different modes labeled by the index $j = \mathrm{I, II, III, IV}$. Obviously, these modes are collective modes of the whole system, not belonging to any single layer. We can then compute the damping rates of all collective 'modes' by $\tilde{\mathbf{D}}_i = \mathbf{M} \cdot \mathbf{D}_i$, where $\mathbf{M} = \begin{pmatrix} \tilde{g}_{\mathrm{I}} & \tilde{g}_{\mathrm{II}} & \tilde{g}_{\mathrm{III}} & \tilde{g}_{\mathrm{IV}} \end{pmatrix}^{\mathrm{T}}$ is the transformation matrix, and $\mathbf{D}_i = \begin{pmatrix} d_{i,1} & d_{i,2} & d_{i,3} & d_{i,4} \end{pmatrix}^{\mathrm{T}}$ and $\tilde{\mathbf{D}}_i = \begin{pmatrix} \tilde{d}_{i,\mathrm{I}} & \tilde{d}_{i,\mathrm{II}} & \tilde{d}_{i,\mathrm{III}} & \tilde{d}_{i,\mathrm{IV}} \end{pmatrix}^{\mathrm{T}}$ with $i = 1, 2$, denote the $d_{i,j}$ of the original modes and the $\tilde{d}_{i,j}$ of the collective modes, respectively. The $d_{i,j}$ parameters are in principle for systems with non-equal inter-layer distances. Here, we assume that their values can be read from figure 6(c), setting h as the averaged value of the inter-layer distance at the side where the EM wave radiates out.

With all these model parameters settled, we can use the simplified CMT formulas equation (7) (with $j = \mathrm{I, II, III, IV}$) to quantitatively compute each transmission peak inside the OTW. We first take an equal-spaced four-layer system ($h_1 = h_2 = h_3 = 8\,\mathrm{mm}$) to check the validity of our theory. Figure 7(a) depicts the wave functions of four collective modes, obtained by diagonalizing the Hamiltonian matrix equation (9). The NF couplings between adjacent layers do indeed make the modes exhibit a 'collective' nature. The solid curves in figures 7(b)–(e) are the transmittance spectra calculated by equation (7) for the four collective modes, which have reproduced the essential features of the considered modes in term of their positions and bandwidths.

[8] The analytical form of eigenvalues of **H** (with mirror symmetry) can be found in section 2 of supplementary data.

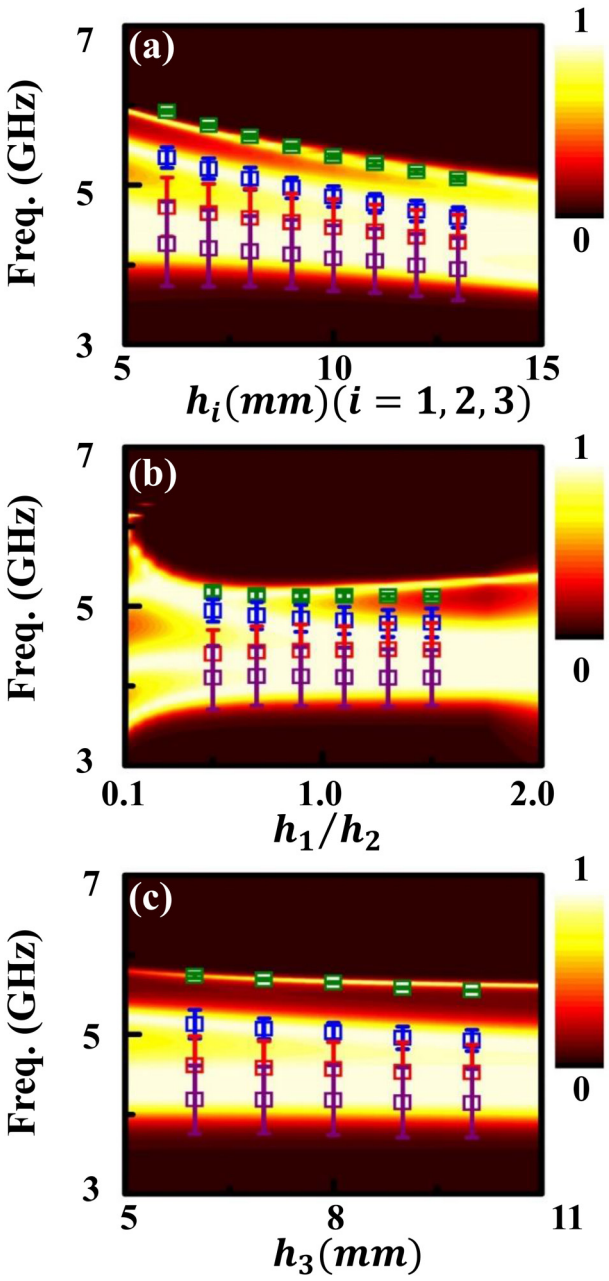

Figure 8. FDTD-computed transmittance spectra of different sets of four-layer systems, with (a) $h_1 = h_2 = h_3$ varying from 5 mm to 15 mm, and (b) varying the h_1/h_2 ratio while keeping $h_1 = h_3$ and total thickness fixed as 36 mm, and (c) varying h_3 alone with $h_1 = 9\,\mathrm{mm}$ and $h_2 = 6\,\mathrm{mm}$ fixed. Here, the symbols and the error bars denote the resonating frequencies and bandwidths of transmission peaks labelled I (purple), II (red), III (blue), and IV (green), calculated with the s-CMT.

The powerfulness of our theory is that it can also reasonably predict the transmission behaviors of systems with *non-equal* inter-layer distances ($h_1 \neq h_2 \neq h_3$), without necessarily performing additional FDTD simulations. We assume that all CMT fitting parameters for such metasurfaces not equally spaced (f_i, $\kappa_{i,j}$, $\kappa'_{i,i}$, $d_{i,j}$) can be determined solely by the local environment. Therefore, they can be approximately obtained from *equal-spaced* CMT parameters by

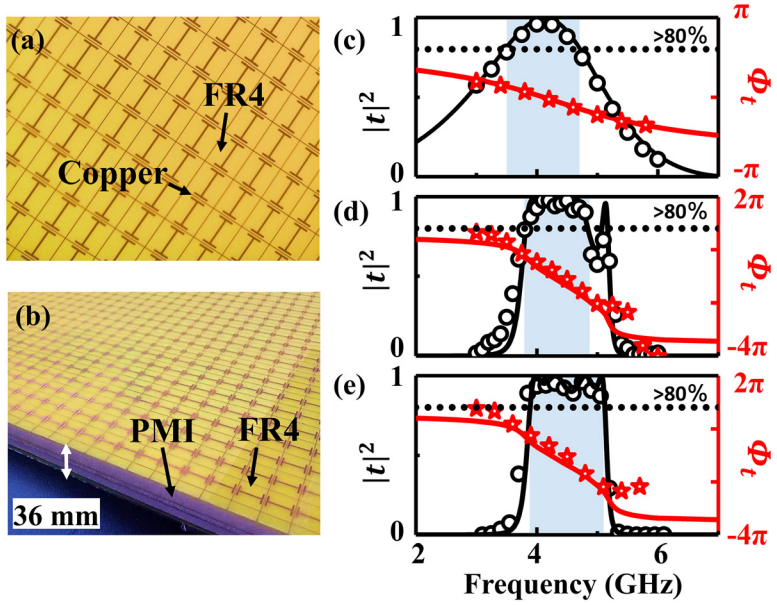

Figure 9. (a) Top view and (b) side view pictures of the fabricated sample. Measured (symbols) and numerical-simulated (curves) transmittance and phase spectra of (c) the single-layer metasurface and the four-layer systems with (d) $h_1 = h_2 = h_3 = 12$ mm and (e) $h_1 = h_3 = 10$ mm, $h_2 = 16$ mm. In our simulations, permittivity of FR4 is set as $\varepsilon_r = 4.3 + 0.01\mathrm{i}$ so as to take the realistic material loss into consideration.

assuming $h = (h_{i-1} + h_i)/2$[9]. Figures 8(a)–(c) depict the CMT-estimated frequencies and bandwidths of the generated transmission peaks, for different series of four-layer systems with equal (figure 8(a)) or non-equal (figures 8(b) and (c)) inter-layer configurations. In all cases studied, we find that our CMT model results are in reasonable agreement with the full-wave simulated spectra, which unambiguously validates our model analysis.

Such nice agreement suggested that we can rely on the *fast* CMT model calculations, rather than the very *time-consuming* full-wave simulations, to optimize the structure in order to design a system exhibiting a flat-band OTW. Specifically, we can vary the inter-layer distances $\{h_i\}$ to control the NF coupling constants $\{\kappa_{ij}\}$, which in turn manipulate the positions and bandwidths of the transmission peaks as desired. The ultimate goal is to find such a configuration $\{h_i\}$ that all transmission peaks inside the OTW can be appropriately jointed together based on the following set of criteria:

$$\tilde{f}_{i+1} - \tilde{f}_i = \tilde{\Gamma}_{i+1} + \tilde{\Gamma}_i, \qquad i = 1, 2, 3. \tag{10}$$

We note that equation (10) is essentially a generalized form of the criterion equation (8) for a two-layer system.

We obtained a configuration based on solving equation (10). The inter-layer distances of the obtained four-layer structure are $h_1 = h_3 = 10\,\mathrm{mm}, h_2 = 16\,\mathrm{mm}$. We then performed microwave experiments to verify our predictions. We fabricated a single-layer metasurface with a 0.5 mm thick FR4 substrate (figure 9(a)), a four-layer equal-spaced system, and a four-layer system with optimized inter-layer distances determined by our theory. We then experimentally measured their transmission spectra. Here, the inter-layer spacers are made of polymethacrylimide (PMI, with $\varepsilon_r = 1.02$) as shown in figure 9(b). In our experiments, we illuminated the sample in a normal manner to *y*-polarized microwaves emitted from a horn antenna placed 1 m away, and then used another horn antenna placed 1 m away from the samples to collect the transmitted signals. Both source and receiver were connected to a vector-field analyzer (Agilent E8362c) so that both the amplitudes and phases of the transmitted signals could be obtained. The open symbols in figure 9(c) are the measured spectra for a single-layer metasurface, and they are in excellent agreement with the FDTD simulations. The transmission spectrum of the equal-spaced four-layer system does show an enlarged transparency window (figure 9(d)), but the inherent transmittance fluctuations at the high-frequency edge shrink the bandwidth of the OTW. In contrast, the four-layer system with an optimized design according to our theory, with a thickness identical to that of its equal-spaced counterpart, does exhibit a quite flat OTW from 3.7 GHz to 5 GHz, as predicted and as shown in figure 9(e).

Before concluding this section, we discuss further the practical implementation of our approach and the key advantages of the strategy. In designing the flat-band OTW structures, the most important task is usually to manipulate appropriately the position of the high-frequency transmission peak, which exhibits a bandwidth much narrower than the inter-mode frequency separation. For example, figure 9(d) shows a transmission dip between the III and IV peaks. Since the established CMT clearly reveals the inherent connections between peak properties and inter-layer couplings (see section 2 in the supplementary data (stacks.iop.org/JPhysD/51/074001/mmedia)), we thus understand how to control these peaks by varying the parameters $\{h_i\}$. Specifically, in order to eliminate the dip between peaks III and IV, we tune both the bandwidth of this peak and the frequency separation between peaks III and IV

[9] Here, when the studied layer is at the side of the whole slab (i.e. layer 1 or layer *N*), we assume *h* just equals the adjacent inter-layer thickness.

by increasing h_2 and decreasing $h_1(=h_3)$ simultaneously, such that the criterion equation (10) can be satisfied. We note that the structure designed by solving equation (10) directly might not be the most optimized, but it can at least serve as a good starting point from which to perform further optimizations. We also emphasize that our design approach, based on the CMT model established, possesses many advantages when compared to the conventional optimization method, and can have a wide range of applications. Our approach is particularly suitable in designing large-N systems with more degrees of freedom. As the number of layers increases, the computational costs of our approach scale *linearly* with N (in calculating the model parameters based on equal-spaced systems), but such costs in a full-wave optimization approach increase much more dramatically. Our approach is not limited to the design of a flat-band OTW, but in principle can be applied to design systems exhibiting other, more complex shapes of transmission spectra (for instance, a double square-wave-like transmission spectrum). We expect that our approach can find many applications in practice.

6. Conclusion

To summarize, we have established a highly efficient approach to the design of optical structures exhibiting desired transmission spectra based on the coupled mode theory. Our analyses reveal that the peaks in the transmission spectrum of a coupled multilayer metasurface are closely related to the 'collective' resonant modes supported by the system, which can be well controlled by the inter-layer couplings. This inherent link enables us to efficiently manipulate the shape of a transmission spectrum by varying the inter-layer distances of the coupled multilayer system. As an illustration of our general theory, we applied it to the design of a structure exhibiting an optical transparency window with a 3.7–5 GHz range with diminished transmittance fluctuations, and demonstrated the idea by microwave experiments. Our design approach is robust, intuitive, fast, and can have many applications in practice.

Acknowledgments

This work is supported by the National Basic Research Program of China (Grant No. 2017YFA0303504), the National Natural Science Foundation of China (Grants Nos. 11704240, 11734007, 11474057, 11404063, and 11674068) and the Natural Science Foundation of Shanghai (Grants Nos. 17ZR1409500, 16ZR1445200, 16JC1403100).

Appendix. Derivations of the transmission coefficients in the coupled mode theory

By applying standard CMT analyses with elegant considerations of time-reversal symmetry and energy conservation [19, 20], we obtain

$$\begin{cases} r_0 d_1^* + t_0 d_2^* = -d_1 & \text{(A.1}a\text{)} \\ t_0 d_1^* + r_0 d_2^* = -d_2 & \text{(A.1}b\text{)} \end{cases}.$$

Here, we assume that $d_1 = |d_1|\,\mathrm{e}^{\mathrm{i}\phi_1}, d_2 = |d_2|\,\mathrm{e}^{\mathrm{i}\phi_2}$. Inserting equation (A.1b) into equation (A.1a), we find that d_1/d_2 can be expressed as

$$\frac{d_1}{d_2} - \frac{d_1^*}{d_2^*} = \frac{t_0}{r_0}\left(1 - \left|\frac{d_1}{d_2}\right|^2\right). \tag{A.2}$$

Further inserting the explicit forms of t_0 and r_0 into equation (A.2), we find that

$$\sin(\Delta\phi) = \frac{f - f_0}{2\Gamma_0}\frac{|\eta|^2 - 1}{|\eta|}, \tag{A.3}$$

where $\Delta\phi = \phi_1 - \phi_2$ is the complex angle of d_1/d_2, and $\eta = d_1/d_2$ describes the asymmetry of the mode's radiation to two different ports. In general, $\Delta\phi$ has two solutions within $0 \sim 2\pi$ when the magnitude of the right side of equation (A.3) is less than 1. In particular, when $|\eta| = 1$, $\Delta\phi$ is found as 0 (π), implying that the mode radiates symmetrically (anti-symmetrically) to two external ports.

Substituting $\Delta\phi$ into equation (A.1) and considering the energy conservation condition $\Gamma_{\mathrm{mode}} = (|d_1|^2 + |d_2|^2)/2$, we obtain

$$\begin{cases} d_1^2 = -\frac{(f-f_0)\mathrm{i}-\eta^*\Gamma_0}{(f-f_0)\mathrm{i}+\Gamma_0}\frac{2}{|\eta|^2+1}\eta\Gamma_{\mathrm{mode}} \\ d_2^2 = -\frac{(f-f_0)\mathrm{i}-\eta^*\Gamma_0}{(f-f_0)\mathrm{i}+\Gamma_0}\frac{2}{|\eta|^2+1}\frac{\Gamma_{\mathrm{mode}}}{\eta} \end{cases}. \tag{A.4}$$

In the limit of $\Gamma_0 \to \infty$, equation (A.4) can be further simplified as

$$\begin{cases} d_1^2 = \frac{2|\eta|^2}{|\eta|^2+1}\Gamma_{\mathrm{mode}} \\ d_2^2 = \frac{2}{|\eta|^2+1}\Gamma_{\mathrm{mode}} \end{cases}, \tag{A.5}$$

which is the essential equation to retrieve the d parameters of multilayer systems. Putting equation (A.5) into (1) and taking the approximation of $\Gamma_0 \to \infty$, we obtain the simplified CMT model for the most general situations (exhibiting asymmetrical radiations to two external ports):

$$t = \frac{2|\eta|}{|\eta|^2+1}\frac{\Gamma_{\mathrm{mode}}}{\mathrm{i}(f - f_{\mathrm{mode}}) + \Gamma_{\mathrm{mode}}}. \tag{A.6}$$

Equation (A.6) shows clearly that the maximum transmission amplitude is equal to $2|\eta|/(|\eta|^2+1)$ at $f = f_{\mathrm{mode}}$, and perfect transmission can happen only in symmetrical cases with $|\eta| = 1$. In general, both Γ_{mode} and $d_{i,j}$ can be retrieved by fitting the FDTD-simulated transmission spectra on realistic structures with equation (A.6).

ORCID iDs

Shulin Sun https://orcid.org/0000-0003-3046-1142
Shiyi Xiao https://orcid.org/0000-0003-3356-4841

References

[1] Sarabandi K and Behdad N 2007 *IEEE Trans. Antennas Propag.* **55** 1239–45

[2] Bayatpur F and Sarabandi K 2008 *IEEE Trans. Microw. Theory Tech.* **56** 774–81
[3] O'Connor B, Haughn C, An K-H, Pipe K P and Shtein M 2008 *Appl. Phys. Lett.* **93** 433
[4] Lee J H, Woo K Y, Kim K H, Kim H-D and Tae G K 2013 *Opt. Lett.* **38** 5055–8
[5] Pfeiffer C and Grbic A 2013 *Appl. Phys. Lett.* **102** 231116
[6] Pfeiffer C and Grbic A 2014 *Phys. Rev. Appl.* **2** 044012
[7] Cheng H, Liu Z, Chen S and Tian J 2015 *Adv. Mater.* **27** 5410–21
[8] Pfeiffer C, Emani N K, Shaltout A M, Boltasseva A, Shalaev V M and Grbic A 2014 *Nano Lett.* **14** 2491–7
[9] Cui Y, Xu J, Hung Fung K, Jin Y, Kumar A, He S and Fang N X 2011 *Appl. Phys. Lett.* **99** 253101
[10] Ding F, Cui Y, Ge X, Jin Y and He S 2012 *Appl. Phys. Lett.* **100** 103506
[11] Wang B X, Wang L L, Wang G Z, Huang W Q, Li X F and Zhai X 2014 *Appl. Phys.* A **115** 1187–92
[12] Liu S, Chen H and Cui T J 2015 *Appl. Phys. Lett.* **106** 151601
[13] Liu N and Giessen H 2010 *Angew. Chem., Int. Ed.* **49** 9838–52
[14] Zhao Y, Belkin M A and Alù A 2012 *Nat. Commun.* **3** 870
[15] Bloemer M, D'Aguanno G, Mattiucci N, Scalora M and Akozbek N 2007 *Appl. Phys. Lett.* **90** 174113
[16] Cai T, Tang S, Wang G, Xu H, Sun S, He Q and Zhou L 2017 *Adv. Opt. Mater.* **4** 1600506
[17] Huang K *et al* 2016 *Laser. Photon. Rev.* **10** 500–9
[18] Glybovski S B, Tretyakov S A, Belov P A, Kivshar Y S and Simovski C R 2016 *Phys. Rep.* **634** 1–72
[19] Haus H A 1984 *Waves and Fields in Optoelectronics* (Englewood Cliffs, NJ: Prentice Hall) pp 197–234
[20] Fan S, Suh W and Joannopoulos J D 2003 *J. Opt. Soc. Am.* A **20** 569–72
[21] Ebbesen T W, Lezec H J, Ghaemi H F, Thio T and Wolff P A 1998 *Nature* **391** 667
[22] Liu H, Genov D A, Wu D M, Liu Y M, Steele J M, Sun C, Zhu S N and Zhang X 2006 *Phys. Rev. Lett.* **97** 243902
[23] Fedotov V A, Rose M, Prosvirnin S L, Papasimakis N and Zheludev N I 2007 *Phys. Rev. Lett.* **99** 147401
[24] Hao F, Larsson E M, Ali T A, Sutherland D S and Nordlander P 2008 *Chem. Phys. Lett.* **458** 262
[25] Francescato Y, Giannini V and Maier S A 2012 *ACS Nano* **6** 1830
[26] Hsu C W, DeLacy B G, Johnson S G, Joannopoulos J D and Soljacic M 2014 *Nano Lett.* **14** 2783–8
[27] Xu H, He Q, Xiao S, Xi B, Hao J and Zhou L 2011 *J. Appl. Phys.* **109** 023103
[28] Xi B, Xu H, Xiao S and Zhou L 2011 *Phys. Rev.* B **83** 165115